Internal Energies of Ion-Sputtered Neutral Tryptophan and Thymine Molecules Determined by Vacuum Ultraviolet Photoionization

Jia Zhou[1], Lynelle K. Takahashi[1,2], Kevin R. Wilson[1], Stephen R. Leone[1,2,3,#], Musahid Ahmed[1]*

[1]*Chemical Sciences Division, Lawrence Berkeley National Laboratory, Berkeley, CA 94720*

[2]*Department of Chemistry, University of California at Berkeley, Berkeley, CA 94720*

[3]*Department of Physics, University of California at Berkeley, Berkeley, CA 94720*

* Corresponding author: MS: 6R-2100, Lawrence Berkeley National Laboratory, 1 Cyclotron Road, Berkeley, CA 94720, USA. Phone: (510) 486-6355; fax: (510) 486-5311; e-mail: MAhmed@lbl.gov

[#]On appointment as a Miller Research Professor in the Miller Institute for Basic Research in Science

Abstract

Vacuum ultraviolet photoionization coupled to secondary neutral mass spectrometry (VUV-SNMS) of deposited tryptophan and thymine films are performed at the Chemical Dynamics Beamline. The resulting mass spectra show that while the intensity of the VUV-SNMS signal is lower than the corresponding secondary ion mass spectroscopy (SIMS) signal, the mass spectra are significantly simplified in VUV-SNMS. A detailed examination of tryptophan and thymine neutral molecules sputtered by 25 keV Bi_3^+ indicates that the ion-sputtered parent molecules have ~2.5 eV of internal energy. While this internal energy shifts the appearance energy of the photofragment ions for both tryptophan and thymine, it does not change the characteristic photoionizaton efficiency (PIE) curves of thymine versus photon energy. Further analysis of the mass spectral signals indicate that approximately 80 neutral thymine molecules and 400 tryptophan molecules are sputtered per incident Bi_3^+ ion. The simplified mass spectra and significant characteristic ion contributions to the VUV-SNMS spectra indicate the potential power of the technique for organic molecule surface analysis.

Keyword: imaging mass spectrometry, vacuum ultraviolet, synchrotron, internal energy, desorption

Introduction

Imaging mass spectrometry, particularly secondary ion mass spectrometry (SIMS), has long been successfully utilized in materials science studies. Recently, however, there has been growing interest in applying this tool to problems of biological relevance.[1, 2] For example, in 2006 lipid domains within prepared lipid membranes were imaged with a spatial resolution of ~100 nm using SIMS,[3] and in 2007 the fate of fixed nitrogen in host cells was mapped using multi-isotope imaging mass spectrometry.[4] A major advantage of imaging mass spectrometry for biological studies is that no sample labeling is required since the chemical species are identified by their masses. Furthermore, in the case of SIMS, the spatial resolution is not restricted by the optical diffraction limit since the desorption source is atomic or molecular ions, yielding images with resolution on the order of tens of nanometers. However, there are also complications arising from this methodology. In particular, SIMS is not a quantitative method because the formation of secondary ions depends strongly on the local environment, i.e. the matrix effect, and the sensitivity for different compounds can vary by orders of magnitude. These make interpreting the resulting images difficult, especially for chemically complex, real-life systems.

Secondary neutral mass spectrometry (SNMS) was developed to access the neutral portion of the ion-sputtered molecules. Compared to SIMS, where the desorption and ionization steps are both initiated by primary ions, SNMS utilizes electrons or photons to postionize the neutral molecules. Because the ionization step is decoupled from the desorption step, SNMS can yield quantitative images.[5] However, due to the high energy needed to ionize most molecules, SNMS experiments typically employ table top lasers via a multiphoton ionization scheme to probe both inorganic and organic samples.[6-9] The excess energy deposited into the molecules during such ionization processes often result in molecular fragmentation, complicating the mass spectrum and limiting the applicability of this

technique.[10] This is further compounded by the fact that the neutral molecules already have a certain amount of internal energy imparted by the sputtering process. To address this issue of dissociative photoionization, it is valuable to determine the amount of internal energy that is present in the ion-sputtered molecules prior to photoionization.

Previous experimental studies have been performed on inorganic surfaces to analyze the energetics of the ion-sputtered atoms and molecules. In particular, in a resonant two-photon ionization experiment, it was determined that Ag_2 clusters sputtered by 5 keV Ar^+ had a vibrational temperature of 2000-3000 K and a rotational temperature of 5000-8000 K.[11] More recently, by comparing photoionization efficiency (PIE) curves of In_n clusters sputtered by 15 keV Xe^+ with those that are in a molecular beam, it was found that the ion-sputtered In_2 clusters have an internal temperature of 4000 K.[12] On the other hand, molecular dynamics simulations show that over organic surfaces some population of the ion-sputtered molecules may remain intact with relatively low internal energy.[13] Therefore, by establishing the extent of internal excitation within these intact ion-sputtered molecules, one can evaluate the applicability of the SNMS technique to various classes of organic compounds.

Recently, we implemented VUV-SNMS at the Chemical Dynamics Beamline at the Advanced Light Source, utilizing tunable vacuum ultraviolet (VUV) radiation from a synchrotron source to perform single photon ionization of the ion-sputtered neutral molecules.[14] Single photon ionization permits a controlled amount of internal energy to be deposited into the molecule,[15] and the wide tunability of a synchrotron photon source allows measurements of photoionization efficiency versus photon energy, which are characteristic of individual chemical species and sensitive to internal energies. Using this technique it is possible to determine the internal energies of the ion-sputtered molecules.[16] In this paper, we report the application of VUV-SNMS to thymine and tryptophan, a DNA base and an amino

acid, respectively, to obtain the typical desorption efficiencies and the observed internal energies of the intact parent molecules.

Experiment

A modified commercial secondary ion mass spectrometer (TOF.SIMS 5, ION-TOF Inc.), operating under ultrahigh vacuum conditions (10^{-9} mbar, 1 mbar = 0.1 kPa), is coupled to the VUV light source on the Chemical Dynamics Beamline at the Advanced Light Source; the setup has been described in detail previously.[14] Briefly, pulses of Bi_3^+ primary ions impact the sample surface at 45°, generating secondary ions and neutrals. The secondary ions and photoionized neutrals are extracted into a reflectron time-of-flight (TOF) mass spectrometer with a two-meter long path length. The SIMS data are acquired with TOF conditions that are optimized for secondary ion detection, while the VUV-SNMS data are acquired with TOF settings optimized for photoion detection.[14] The samples of thymine and tryptophan used in this experiment are purchased from Sigma Aldrich (both ≥99% purity), deposited by suspending in methanol and spin coated onto silicon substrates. The samples are analyzed without sputter-cleaning to avoid unnecessary damage to the organic surfaces. Each analysis is performed in an area of 150 x 150 μm^2, with a 64 pixel x 64 pixel raster. The thymine data were acquired with a 260 μs cycle time, equivalent to a 3.8 kHz repetition rate, and the tryptophan data were acquired with a 280 μs cycle time.

The undulator-based beamline, described in detail elsewhere,[17] generates wavelength-tunable, quasi-continuous (500 MHz) VUV light. The synchrotron was recently upgraded to operate in top-off mode,[18] increasing the photon flux available to each beamline. The spectral resolution of the synchrotron output used in this work is determined to be 0.2 eV by measuring the full width at half maximum (FWHM) of the autoionizing resonance of ion-sputtered silicon atoms at 9.8 eV. Argon is used in the gas filter to remove higher harmonics from the undulator emission. Also situated in the gas filter is a small (100 μm) horizontal slit that narrows the vertical height of the VUV beam, delivering ~10^{15}

photons/s to the apparatus with a spot size of approximately 200 μm (vertical) x 600 μm (horizontal). Photon flux curves as a function of energy are determined using a NIST-calibrated photodiode (SXUV-100, International Radiation Detectors) attached to the light exit port.

Due to the non-conductive nature of the organic surfaces studied here, a new ion extraction scheme is utilized to enhance the detection of photoionized secondary neutrals. Figure S-1 depicts the main pulsed extraction schemes that are used. Typically, in the positive ion mode, a 10 μs long -2000 V pulse is applied to the extractor with 0 μs delay (Figure S-1a). In this case, the extractor is at -2000 V when the bismuth ion pulse impacts the surface, resulting in an extraction scheme that is the same as DC extraction for the secondary ions and neutrals; the advantage is that the background signal arising from the VUV ionization of background gas is significantly reduced since the ions are not being continuously extracted into the TOF. Another possible extraction scheme is to delay the extraction pulse with respect to the bismuth pulse such that the extractor sits at ground potential when the bismuth ion pulse impacts the surface (Figure S-1b). This pulsing scheme is advantageous because it improves the mass resolution of VUV-SNMS signal, since it allows for the accumulation of photoionized molecules in the extraction region before the voltage pulse is applied. This improved mass resolution, as illustrated in Figure S-2, is a necessary feature when analyzing organic samples. The major disadvantage of this scheme is that the secondary ions and the photoionized secondary neutrals have very similar flight paths through the TOF, making suppression of secondary ions difficult. Furthermore, the electrically insulating organic surface can cause the secondary ion signal to fluctuate from scan to scan, which significantly complicates the separation of VUV-SNMS signal from the secondary ion background. Therefore, a double extraction pulse scheme (Figure S-1c) is used for the organic samples studied here. The first pulse is used to extract the prompt secondary ions; due to the short duration of this pulse, only a small mass range of secondary ions can reach the detector, reducing the secondary ion background. Because most of the secondary neutrals are not yet photoionized during this first pulse, they are

unaffected in their initial trajectory. The second pulse acts as the normal delayed extraction pulse for the photoionized secondary neutrals. While some secondary ions still reach the detector with this extraction scheme, it is possible to adjust the timing such that the mass range of interest can be relatively free of background signal.

Computational Details

Geometry optimization and vibrational frequency calculations are carried out for tryptophan, thymine and their fragments at the B3LYP level with the 6-311+G(d,p) basis set using the Gaussian 03 program.[19] Relative energies and ionization energies are obtained by subtracting the computed energy of the final state from the initial state, including the zero-point energy corrections. For thymine, the Gaussian 03 output files are used in the FCFGAUS program of Ervin *et al.*[20] for the Franck-Condon simulation, in which the Duschinsky rotation matrix and the displacement vectors are calculated. The resulting simulated photoelectron spectrum is visualized with the PESCAL[21] program.

For the simulation of PIE curves of the diatomic metal clusters, a Mathcad program is used to solve the Schrodinger equation for the vibrational potential using the 1-dimensional DVR (discreet variable representation) method.[22] Morse potentials are calculated for the neutral and cation dimers using experimental values when available,[23, 24] and theoretical values otherwise (Au_2 and As_2 cations are calculated at the CCSD(T) level with cc-pVTZ-pp[25] and cc-pVTZ basis sets, respectively, using the Gaussian 03 program[19]). A total of 300 particle-in-a-box basis sets are used for the simulation, and the resulting wave functions for the initial state (neutral dimer) and final state (cation dimer) are used to calculate the Franck-Condon factors. The simulated photoelectron spectrum is integrated to give the PIE curve. The results are convoluted with a Gaussian width of 2700 cm^{-1}, corresponding to the resolution of the VUV light used for the experimental PIE curves. The Boltzmann distribution for the vibrational population of the initial state is included to simulate the PIE curves for various vibrational temperatures.

Results and Discussion

Mass Spectra of Organic Molecules

VUV-SNMS signals are observed in our laboratory recently for numerous organic samples, e.g. polycyclic aromatic hydrocarbons (coronene, chrysene, etc.), amino acids (phenylalanine, asparagine, etc.), various DNA bases, and other biologically-relevant compounds such as coniferyl alcohol, a component of lignin. However, for the purpose of analyzing internal energies of ion-sputtered molecules, only two compounds, tryptophan and thymine, are discussed here. Shown in Figures 1 and 2 are the VUV-SNMS mass spectra of thymine and tryptophan acquired at various photon energies ranging from 8 eV to 10 eV, as well as the corresponding SIMS mass spectra; the SIMS and VUV-SNMS of each sample are acquired over the same area on the sample surface to minimize variations. The VUV-SNMS mass spectra of thymine show a dominant feature at m/z = 126, corresponding to the thymine parent, and its photon energy dependence agrees well with the ionization onset of thymine at 8.9 eV.[26] An additional feature at m/z = 55 is visible at 10 eV and 9.5 eV photon energy (Figures 1a and 1b, respectively), which corresponds to the $C_3H_5N^+$ fragment of thymine. The VUV-SNMS mass spectra of tryptophan, on the other hand, show only one predominant feature at the fragment mass of m/z = 130 for all photon energies. The SIMS mass spectra of thymine and tryptophan are generally more complicated, but for both species there is a relatively strong feature at the protonated parent mass.

Comparing the SIMS data to the VUV-SNMS data, one can see that each technique has an advantage over the other. SIMS shows a higher signal count with fewer bismuth ions used, albeit the protonated parent is favored over the parent in SIMS; VUV-SNMS has a simpler mass spectrum, with all dominant features easily assignable. The difference between the signal counts of the two methods is related to the difference in the ionization cross sections. In SIMS, the protonated parent is most likely formed through the collision of neutral molecules with cationic species that are generated by the very

energetic desorption process. This "ionization" cross section is poorly quantified, and it can vary significantly depending on the local environment of the surface. On the other hand, in VUV-SNMS the photoions, e.g. for thymine, are formed from single photon ionization of the neutral thymine molecules. The photoionization cross section and branching fractions are well defined, making the signals depend, for the most part, only on the photon flux, the photon energy, and the desorption yield. Thus the comparatively lower signal count rate in VUV-SNMS is due to the cross section and the low peak power of the quasi-cw synchrotron source.

In terms of the number of spectral features present, a dramatic difference can be seen between the VUV-SNMS and SIMS mass spectra of tryptophan. The SIMS mass spectrum (Figure 2d) exhibits many features, with a cluster of intense peaks every ~10 mass units, up to the protonated parent signal. The VUV-SNMS mass spectrum of tryptophan, on the other hand, is very simple. There is one dominant peak at m/z = 130, corresponding to the characteristic methylene indole cation fragment produced by dissociative photoionization. The difference in the mass spectra between VUV-SNMS and SIMS is well illustrated in this case. Many of the SIMS mass spectral artifacts, such as disproportionately strong Na^+ and K^+ signals and the ever-present hydrocarbon envelope at low masses, are not present in the VUV-SNMS mass spectrum. This improvement over SIMS would be a great advantage when studying complex and chemically heterogeneous organic surfaces.

Desorption Yield

The neutral desorption yield can be estimated from the observed photoion intensity because VUV-SNMS utilizes well-defined ionization processes. Using the linear approximation of Beer's law, the number of neutral thymine molecules sputtered per second, N, is related to the number of thymine photoions observed per second, Z, by:[14]

$$N \cong \frac{Z}{0.08\sigma F\tau}\,. \qquad (1)$$

The factor of 0.08 is the previously determined detection efficiency of the VUV-SNMS instrument measured with xenon.[14] The photoionization cross section of thymine, σ, is estimated to be ~20 Mb (1 Mb = 1 x 10^{-18} cm^2) at 10 eV photon energy, based on the experimental photoionization cross section of aromatic systems.[27] The average photon flux in the interaction region, F, is measured to be 1.2 x 10^{18} photons/(cm^2·s) at 10 eV. The average time that each neutral thymine molecule spends in the VUV beam path, τ, is calculated assuming a typical kinetic energy of 1.5 eV[28] for the ion-sputtered thymine molecules, which yields a travel time of 0.2 μs through the measured 200 μm vertical FWHM of the VUV beam. The 10 eV VUV-SNMS mass spectrum shown in Figure 1a is acquired with 50 ns pulses of Bi_3^+ for 27 seconds at a 3.85 kHz repetition rate, resulting in 950 ion counts for thymine. From Equation 1, this would yield 9.2 x 10^7 neutral thymine molecules per second. The 50 ns pulses of Bi_3^+ running at 260 μs cycle time has a beam current of 0.38 pA, corresponding to 2.4 x 10^6 Bi_3^+ per second. Together, the estimated desorption yield is ~40 thymine molecules per Bi_3^+ ion for the dataset presented in Figure 1a. The VUV-SNMS image of thymine parent, also shown in Figure 1a, indicates that the organic surface is not uniform, despite the attempt to spin coat the sample uniformly; this is largely due to the fact that thymine does not dissolve well in methanol. As the image shows, thymine covers ~50% of the substrate surface. This means that only ~50% of the incident Bi_3^+ would result in useful yield. Taking this into account, the corrected estimated desorption yield of thymine is then ~80 neutral thymine molecules per incident Bi_3^+ ion.

A similar analysis can be applied to the tryptophan data acquired at 10 eV photon energy, shown in Figure 2a, where the m/z = 130 feature is a well-known cation fragment of tryptophan cation.[29] Using an estimated photoionization cross section of 60 Mb at 10 eV photon energy,[27] the observed 12000 counts of the m/z = 130 photoion in 17 seconds (280 μs cycle time or 3.57 kHz repetition rate)

correspond to 6.1 x 10^8 tryptophan molecules per second, or ~280 tryptophan molecules sputtered per Bi_3^+ for the dataset presented in Figure 2a. The VUV-SNMS image of the m/z = 130 cation, also shown in Figure 2a, indicates that tryptophan has better substrate coverage than thymine, although it is still not uniform. Given the ~70% organic presence in the analyzed area, the corrected estimated desorption yield of tryptophan is ~400 neutral tryptophan molecules per incident Bi_3^+ ion.

There are several experimental parameters and associated uncertainties that should be taken into account when considering the derived desorption yields. In particular, there is no experimental absolute photoionization cross sections for thymine and tryptophan in the photon energy range studied here, hence the estimated values for the ionization cross sections may be inaccurate, although they should be correct within an order of magnitude. The substrate coverage variations of the organic samples do cause differences in the total signal detected from spot to spot. When taking this into account, the desorption yields from several different spatial areas of analysis present consistent values with ± 20% deviations. This fluctuation in signal also includes changes in the Bi_3^+ flux and other minor differences in the samples such as surface contaminants and thickness. Furthermore, there are also systematic errors in the estimated desorption yield. For instance, because the photoionized molecules are delay extracted, some of the ion-sputtered molecules that have higher kinetic energies would leave the extraction region before they can be pulsed into the TOF. This would favor the detection of lower kinetic energy molecules and would decrease the signal count. Also, in the case of thymine, any photo-induced fragmentation is not accounted for, which would again decrease the estimated desorption yield. This may account for the difference in the calculated desorption yield between thymine and tryptophan, as the former is derived from the detected parent signal alone and the latter is derived from the dominant photofragment.

The neutral desorption yield of thymine can also be compared to the protonated thymine signal observed in the SIMS mass spectrum. In Figure 1e, the SIMS spectrum, acquired with 12.5 ns pulses of Bi_3^+ at a repetition rate of 3.85 kHz in 27 seconds, has 23000 counts of protonated thymine. This is equivalent to 1.4 x 10^{-3} protonated thymine ions per incident Bi_3^+ ion. This value is at least 4 orders of magnitude less than the neutral thymine desorption yield calculated from VUV-SNMS over the same area, especially considering that the SIMS mass spectrum is acquired with non-delayed extraction and most likely has higher detection efficiency. This difference in yields highlights the advantage of accessing the neutral species in the desorption plume.

Internal Energies

Previous experiments[14] with VUV-SNMS over metal samples revealed that the PIE curves for both Au_2 and As_2 clusters display lower ionization onsets when compared to reference values. This shift is attributed to vibrational excitation in the neutral clusters imparted by the desorption process. Because there is only one vibrational mode in these dimers, a relatively simple simulation, as outlined in the computational details section, can be performed to extract the vibrational temperature of the neutral clusters. The simulated PIE curves for Au_2 and As_2 are compared to VUV-SNMS PIE curves previously obtained[14] with Bi_3^+ primary ions in Figure 3. The 0-0^+ transitions in the simulated PIE curves are fixed to experimentally-determined ionization onsets,[30, 31] leaving the intensity as the only adjustable parameter in the fit between VUV-SNMS PIE curves and simulated PIE curves. As Figure 3 shows, the simulations fit very well with the experimental data for both Au_2 and As_2 when vibrational temperatures of 5000 K and 4000 K, respectively, are used. Although the uncertainties in these values are high because there are only subtle differences in the simulated PIE curves in this temperature range, they nonetheless demonstrate the approximate amounts of internal energy imparted to the sputtered

neutral metal clusters by the primary ion impact. These vibrational temperatures are also in good agreement with previous studies on other metal clusters.[11, 12]

There is one major difference between organic molecules and the metal clusters that have been studied thus far, namely, the number of internal degrees of freedom available to the system. Organic molecules in the mass range of 100 to 200 daltons can have up to 100 or more vibrational modes, which at a temperature of 5000 K would correspond to tens of eV in internal energy. In comparison, Au_2 at the same temperature has only 0.4 eV of internal energy. Therefore, it is not straightforward to draw conclusions for organic systems based upon the results of the metal systems. In order to have a better grasp of the internal energy in ion-sputtered organic molecules, we turn to the VUV-SNMS results of tryptophan and thymine.

Shown in Figure 4 is the VUV-SNMS mass spectrum of tryptophan acquired with 8.25 eV photon energy. The insert gives a closer view of the spectral range around the parent mass at m/z = 204. The signal intensity for the parent mass is obviously much weaker than the intensity of the dominant fragment at m/z = 130. Nevertheless, the ratio between the two can be used to estimate the internal temperature of the ion-sputtered tryptophan. Wilson *et al.*[32] carried out an experiment at the Chemical Dynamics Beamline wherein they measured the temperature dependence of the parent-to-fragment ratio of tryptophan at 8.25 eV photon energy by desorbing the molecules from an aerosol particle by collisions with a heated target. Their results show that in the temperature range from 373 K to 573 K, the parent-to-fragment ratio of tryptophan has an exponential dependence on temperature. This well-defined dependence allows us to extrapolate the Wilson *et al.*[32] data to the ratio of 0.008 observed in the present VUV-SNMS mass spectrum. Shown in Figure S-3 is the extrapolation plot, and from this we estimate the internal temperature of ion-sputtered tryptophan to be 850 K.

To better understand the implications of this internal temperature, theoretical calculations as outlined in the computational details section are carried out for tryptophan and its fragments. Figure 5 illustrates the structures and relative energies of the tryptophan cation (m/z = 204) and the dominant fragments (m/z = 130 and m/z = 74). The fragmentation pathway that results in the formation of the m/z = 130 cation involves the cleavage of a C-C bond, indicated by the arrow in Figure 5, that connects the amino acid moiety to the indole rings.[29] Upon fragmentation, the charge remains on the methylene indole fragment, producing the observed m/z = 130 feature, while the neutral fragment, the deprotonated glycine with a mass of 74, is not detected. The calculated energy of the fragments is 1.15 eV higher than the calculated energy of the radical tryptophan cation, suggesting that at least 1.15 eV is needed to break the indicated bond when the tryptophan cation is in the ground state. Previous experiments by Wilson *et al.*[32] showed that the methylene indole fragment has an appearance energy of 8 eV at 373 K. The average vibrational energy of tryptophan at 373 K can be approximated by treating its vibrations as a collection of harmonic oscillators,[32] giving

$$E_{vib} = \sum_{i=1}^{s} \frac{h\nu_i}{e^{h\nu_i/kT} - 1} . \qquad (2)$$

Thus, the vibrational energy of tryptophan at 373 K is calculated to be 0.44 eV. Together with the 7.2 eV ionization energy of tryptophan,[33] the 8 eV appearance energy of the methylene indole fragment indicates that the fragmentation starts at 1.2 eV above the tryptophan cation ground state. This is in good agreement with the calculated 1.15 eV minimum energy needed for fragmentation.

As discussed above, the parent-to-fragment ratio of the VUV-SNMS data indicates that the ion-sputtered tryptophan molecules have a much higher average temperature of 850 K. From Eq. 2, this temperature corresponds to 2.2 eV of internal vibrational energy. The 8.25 eV ionizing photon already puts the tryptophan cation 1 eV above its ground state; together with this 2.2 eV internal vibrational

energy, the tryptophan cation has an excess of 3 eV in internal energy. Given that the dissociation limit is only 1.15 eV above the ground state, it is not surprising then that the VUV-SNMS mass spectrum of tryptophan is dominated by the methylene indole cation fragment.

In order for the preceding discussion on the tryptophan energetics to be valid, we must validate the assumption that the m/z = 130 feature observed in the VUV-SNMS spectrum is the result of dissociative photoionization and not due to the photoionized neutral fragment. There are two major channels of formation for the neutral methylene indole radical—directly from the surface via the ion-sputtering process and fragmentation of metastable tryptophan molecules above the surface. In the first case, collisions involving the open-shell reactive methylene indole radicals near the surface should also lead to the formation of neutral methyl indole (m/z = 131). However, a comparison with the expected isotopic distribution of methylene indole, shown in Figure 6, indicates that the m/z = 131 feature is due to the heavier isotopes of C_9H_8N and not from methyl indole (methyl indole has an ionization energy of 7.5 eV[34] and methylene indole has a calculated ionization energy of 6.2 eV). If the methylene indole radicals instead originate from fragmentation of metastable ion-sputtered tryptophan molecules, a mass spectral feature at m/z =74 should be observed as well, corresponding to the photoionized deprotonated glycine, for which the calculated ionization energy is 7.4 eV. Figures 6a and 6b show that, at both 10 eV and 8 eV photon energies, there is no major feature at m/z = 74 in the mass spectra. Therefore, the lack of any significant m/z = 74 and 131 features support the assumption that the m/z = 130 feature in the VUV-SNMS mass spectra is predominantly due to dissociative photoionization of intact neutral tryptophan molecule.

The VUV-SNMS results indicate that the intact neutral tryptophan molecules, sputtered by 25 keV Bi_3^+ primary ions, possess an internal temperature of ~850 K, which is equivalent to a vibrational energy of ~2.2 eV. Unfortunately, because the methylene indole fragment and the parent tryptophan

signals differ in intensities by two orders of magnitude, we cannot ascertain the error bars on the derived 850 K internal temperature. Particularly, while we can establish the fragmentation pathway that yields the methylene indole cation, we cannot be certain that there are no minor fragmentation pathways that would reduce the parent signal without affecting the m/z = 130 signal. Further uncertainties also arise from the poor signal-to-noise ratio of the weak tryptophan photoion signal as well as the large extrapolation of the Wilson *et al.*[32] data. Therefore, we now turn to the VUV-SNMS data on thymine to examine if the ion-sputtered thymine molecules also contain similar internal energies.

Dissociative photoionization of gas phase thymine has been previously studied using VUV photons.[35] It has been found that the dominant cation fragment at m/z = 55 is formed via a multi-step fragmentation pathway:[36]

$$C_5H_6N_2O_2^+ \xrightarrow{-HNCO} C_4H_5NO^+ \xrightarrow{-CO} C_3H_5N^+ \quad (3)$$

Such a complex reaction pathway cannot be simply explained by comparing the energetics at the dissociation limit. Fortunately, there are experimental values to draw upon. Jochims *et al.*[35] found that the $C_4H_5NO^+$ cation at m/z = 83, although very weak, does have an appearance energy of 10.7 eV, which is 1.9 eV above their experimentally observed ionization onset of thymine at 8.8 eV. The dominant cation fragment, $C_3H_5N^+$ at m/z = 55, has an appearance energy of 11.7 eV, 2.9 eV above the thymine ionization energy. In Figure 1b, a peak can be seen emerging at m/z = 55 in the VUV-SNMS mass spectrum acquired with 9.5 eV photon energy. Given the ionization energy of thymine, this result would imply that the 25 keV Bi_3^+ ion-sputtered thymine has an internal energy of 2.4 ± 0.3 eV; the large error bar is because of the uncertainty in the onset of the fragment feature due to SIMS background in that spectral region. For thymine, this internal energy corresponds to a vibrational temperature of ~1300 K, derived using Eq. 2, which is significantly higher than the tryptophan vibrational temperature. This indicates that the ion-sputtered tryptophan and thymine share a similar internal energy of ~2.5 eV,

rather than a similar internal temperature. These values are quite different than the internal energies and temperatures that have been obtained for the metals systems as discussed earlier, and given that thymine and tryptophan have different functional groups, number of atoms and number of vibrations, the fact that these two molecules share a similar internal energy may be a reflection on the nature of the ion-sputtering process on organic surfaces.

Figure 1 shows that the dominant feature in the VUV-SNMS of thymine is the parent signal, from which, PIE curves for the ion-sputtered thymine molecules can be obtained. The average of four VUV-SNMS PIE curves of thymine, normalized to each other at 9.2 eV, is shown in Figure 7a, where the grey shading indicates fluctuations in the four individual scans. For comparison purposes, shown in Figure 7b is the average of two PIE curves also acquired with the TOF.SIMS 5 instrument, utilizing the heating/cooling stage to thermally vaporize thymine samples for VUV photoionization. The difference between Figures 7a and 7b lies only in the method of desorption, 25 keV Bi_3^+ ions vs. 40 °C thermal desorption. While the VUV-SNMS PIE curves are noisier than the thermal desorption PIE curves, it is nonetheless evident that there is no significant shift in the ionization onset between Figures 7a and 7b. The ion-sputtered thymine molecules have an internal energy of ~2.5 eV, corresponding to ~1300 K in vibrational temperature, while the thermal desorption is performed at 40 °C. The difference in the ionization onset between the two averaged PIE curves is only 0.1 eV, which is within the energy resolution of the VUV light. This similarity can be understood from the computed photoelectron spectrum of thymine at 0 K, shown in Figure 8. The Franck-Condon simulation indicates that neutral thymine does not have a large geometry change upon ionization, resulting in the $0\text{-}0^+$ origin transition being the dominant feature in the simulated photoelectron spectrum. Therefore, even if there is extensive vibrational excitation, the dominant transitions upon ionization would be the sequence bands. Any changes in the ionization onset would mostly be due to differences in the vibrational frequencies and anharmonicity effects, which would not result in drastic shifts in the onset. Although it would be

possible to carry out a simulation of the experimental PIE curves of thymine, the numerous vibrational modes present make such a simulation beyond the scope of the present study.

Recently, Garrison *et al.*[13] performed molecular dynamics simulations of 20 keV C_{60}^{+} bombardment of an octane surface. They found that the sputtered molecules vary in internal energy by their distance away from the primary ion impact site, and the molecules with higher internal energies appear to leave the surface first with higher kinetic energy. In terms of our experiment, the double pulse extraction scheme may cause the results to be biased toward the lower internal energy population. Nonetheless, the results from the current study provide a good guide for future endeavors in SNMS studies. For example, the observed ~2.5 eV internal energy explains why SNMS methods have worked well for polyaromatic hydrocarbons where the pi-conjugated bonding system stabilizes the molecules from fragmentation. It also explains why, for molecules whose fragmentation pathways involve single bond breakage, which is the case for many amino acids, it is often the characteristic fragments that are observed in the resulting mass spectrum. For the larger long chain hydrocarbons, where both SIMS and SNMS experiments have not fared well, this internal energy is something that has to be minimized in some way before meaningful results can be obtained. With this ability to examine systematically the internal energy of the ion-sputtered molecules, VUV-SNMS can aid in the further refinement of desorption techniques while at the same time provide complementary and quantitative information and is a valuable new tool in imaging mass spectrometry.

Conclusions

VUV-SNMS studies over organic surfaces have been carried out at the Chemical Dynamics Beamline. The resulting mass spectra show that while the intensity level of the VUV-SNMS signal is lower than the corresponding SIMS signal, the mass spectra are significantly simpler. The relatively low VUV-SNMS signal is a direct result of the limited flux of the quasi-cw (500 MHz) synchrotron source,

coupled with the fact that majority of the photons are not used as the instrument operates at 1-10 kHz repetition rate; this highlights the need for a higher peak power next generation light source.[37, 38] Analysis shows that the organic samples have a neutral desorption yield of ~80 thymine molecules sputtered per incident Bi_3^+ and ~400 tryptophan molecules sputtered per incident Bi_3^+. A detailed examination of the observed energetics of tryptophan and thymine indicates that the ion-sputtered neutral molecules have ~2.5 eV internal energy. While this internal energy can shift the appearance energy of the fragments from dissociative photoionization, it may not necessarily change the characteristic PIE curves of the molecules, depending on the Franck-Condon window for photoionization. This means that for certain chemical species, excessive internal energy in the neutral molecules may result in dissociative photoionization at the minimal photon energy needed for ionization. Nonetheless, by controlling the amount of energy imparted to the ion-sputtered molecules in the ionization step, it should be possible to minimize fragmentation even though completely elimination of fragmentation may not be possible in certain cases. This would lead to much simpler mass spectra that are easier to assign, which is the first step towards successful wide application of imaging mass spectroscopy on heterogeneous organic systems such urban aerosols and lignocellulosic systems.

Acknowledgements

The authors would like to thank Prof. Ricardo Metz for providing the Mathcad program to simulate the PIE curves of the metal systems and for helpful discussions. We would also like to thank Corey Foster (ION-TOF Inc.) for his continuing technical assistance. This work was supported by the Director, Office of Energy Research, Office of Basic Energy Sciences, and Chemical Sciences Division of the U.S. Department of Energy under contracts No. DE-AC02-05CH11231.

Supporting Information Available:

Figures (S1-3) showing various pulsed extraction schemes used in this work, effects of varying the pulsed delay, and temperature dependence of the parent-to-fragment ratio of tryptophan are available as supplementary information. This material is available free of charge via the Internet at http://pubs.acs.org.

References

(1) Heeren, R. M. A.; Smith, D. F.; Stauber, J.; Kukrer-Kaletas, B.; MacAleese, L. *J. Am. Soc. Mass Spectrom.* **2009**, *20*, 1006-1014.
(2) Vickerman, J. C. *Surf. Sci.* **2009**, *603*, 1926-1936.
(3) Kraft, M. L.; Weber, P. K.; Longo, M. L.; Hutcheon, I. D.; Boxer, S. G. *Science* **2006**, *313*, 1948-1951.
(4) Lechene, C. P.; Luyten, Y.; McMahon, G.; Distel, D. L. *Science* **2007**, *317*, 1563-1566.
(5) Kollmer, F.; Bourdos, N.; Kamischke, R.; Benninghoven, A. *Appl. Surf. Sci.* **2003**, *203*, 238-243.
(6) Mollers, R.; Terhorst, M.; Niehuis, E.; Benninghoven, A. *Org. Mass Spectrom.* **1992**, *27*, 1393-1395.
(7) Muller, U.; Schittenhelm, M.; Schmittgens, R.; Helm, H. *Surf. Interface Anal.* **1999**, *27*, 904-910.
(8) Terhorst, M.; Mollers, R.; Niehuis, E.; Benninghoven, A. *Surf. Interface Anal.* **1992**, *18*, 824-826.
(9) Willingham, D.; Kucher, A.; Winograd, N. *Chem. Phys. Lett.* **2009**, *468*, 264-269.
(10) Willey, K. F.; Vorsa, V.; Braun, R. M.; Winograd, N. *Rapid Commun. Mass Spectrom.* **1998**, *12*, 1253-1260.
(11) Wucher, A. *Phys. Rev. B* **1994**, *49*, 2012-2020.
(12) Wucher, A.; Staudt, C.; Neukermans, S.; Janssens, E.; Vanhoutte, F.; Vandeweert, E.; Silverans, R. E.; Lievens, P. *New J. Phys.* **2008**, *10*, 103007.
(13) Garrison, B. J.; Postawa, Z.; Ryan, K. E.; Vickerman, J. C.; Webb, R. P.; Winograd, N. *Anal. Chem.* **2009**, *81*, 2260-2267.
(14) Takahashi, L. K.; Zhou, J.; Wilson, K. R.; Leone, S. R.; Ahmed, M. *J. Phys. Chem. A* **2009**, *113*, 4035-4044.
(15) Hanley, L.; Zimmermann, R. *Anal. Chem.* **2009**, *81*, 4174-4182.
(16) Hoogerbrugge, R.; Bobeldijk, M.; Kistemaker, P. G.; Los, J. *J. Chem. Phys.* **1988**, *88*, 5314-5322.
(17) Heimann, P. A.; Koike, M.; Hsu, C. W.; Blank, D.; Yang, X. M.; Suits, A. G.; Lee, Y. T.; Evans, M.; Ng, C. Y.; Flaim, C.; Padmore, H. A. *Rev. Sci. Instrum.* **1997**, *68*, 1945-1951.
(18) Byrd, J. M. *Nucl. Instrum. Methods Phys. Res. Sect. A-Accel. Spectrom. Dect. Assoc. Equip.* **1999**, *427*, 614-621.
(19) Frisch, M. J., et al. *GAUSSIAN 03*; Gaussian, Inc.: Wallingford CT, 2004.
(20) Ervin, K. M.; Ramond, T. M.; Davico, G. E.; Schwartz, R. L.; Casey, S. M.; Lineberger, W. C. *J. Phys. Chem. A* **2001**, *105*, 10822-10831.
(21) Ervin, K. M. *Fortran PESCAL* **2004**.
(22) Metz, R. B. Ph. D. Thesis, University of California, Berkeley, Berkeley, 1991.
(23) http://www.webbook.nist.gov/chemistry.
(24) Lombardi, J. R.; Davis, B. *Chem. Rev.* **2002**, *102*, 2431-2460.
(25) Schuchardt, K. L.; Didier, B. T.; Elsethagen, T.; Sun, L. S.; Gurumoorthi, V.; Chase, J.; Li, J.; Windus, T. L. *J. Chem. Inf. Model.* **2007**, *47*, 1045-1052.
(26) Choi, K. W.; Lee, J. H.; Kim, S. K. *J. Am. Chem. Soc.* **2005**, *127*, 15674-15675.

(27) Zhou, Z.; Xie, M.; Wang, Z.; Qi, F. *Rapid Commun. Mass Spectrom.* **2009**, *23*, 3994-4002.
(28) Solomko, V.; Delcorte, A.; Garrison, B. J.; Bertrand, P. *Appl. Surf. Sci.* **2004**, *231*, 48-53.
(29) MacLennan, M. S.; Sutherland, K. N.; Orlova, G. *J. Mol. Struct. THEOCHEM* **2007**, *822*, 21-27.
(30) Cheeseman, M. A.; Eyler, J. R. *J. Phys. Chem.* **1992**, *96*, 1082-1087.
(31) Yoo, R. K.; Ruscic, B.; Berkowitz, J. *J. Chem. Phys.* **1992**, *96*, 6696-6709.
(32) Wilson, K. R.; Jimenez-Cruz, M.; Nicolas, C.; Belau, L.; Leone, S. R.; Ahmed, M. *J. Phys. Chem. A* **2006**, *110*, 2106-2113.
(33) Campbell, S.; Beauchamp, J. L.; Rempe, M.; Lichtenberger, D. L. *Int. J. Mass Spec. Ion Proc.* **1992**, *117*, 83-99.
(34) Hager, J. W.; Wallace, S. C. *Anal. Chem.* **1988**, *60*, 5-10.
(35) Jochims, H. W.; Schwell, M.; Baumgartel, H.; Leach, S. *Chem. Phys.* **2005**, *314*, 263-282.
(36) Improta, R.; Scalmani, G.; Barone, V. *Int. J. Mass. Spectrom.* **2000**, *201*, 321-336.
(37) Khan, S. *J. Mod. Opt.* **2008**, *55*, 3469-3512.
(38) http://newscenter.lbl.gov/feature-stories/2009/12/21/accelerators-tomorrow-part1/.

Figure Captions:

Figure 1: VUV-SNMS of thymine (50 ns of Bi_3^+, 25 scans) acquired at photon energies of 10 eV (a), 9.5 eV (b), 9 eV (c) and 8.2 eV (d). For comparison, the SIMS spectrum (12.5 ns of Bi_3^+, 25 scans) acquired over the same area is shown in panel (e). The VUV-SNMS spectra are acquired with TOF conditions optimized for photoion detection; the SIMS spectrum is acquired with TOF conditions optimized for secondary ion detection. In the VUV-SNMS spectra, the m/z = 126 feature corresponds to the thymine parent signal, while the m/z = 55 is the dominant cation fragment. The noise in the spectra around m/z = 50 is due to fluctuations in the SIMS background. In panel (a) also shown is an image of the m/z = 126 feature, showing the spatial distribution of thymine (150 x 150 μm^2, 64 pixel x 64 pixel raster). The SIMS mass spectrum shows a strong signal at m/z = 127, corresponding to protonated thymine.

Figure 2: VUV-SNMS of tryptophan (50 ns of Bi_3^+, 15 scans) acquired at photon energies of 10 eV (a), 9 eV (b) and 8 eV (c). For comparison, the SIMS spectrum (12.5 ns of Bi_3^+, 15 scans) acquired over the same area is shown in panel (d). The VUV-SNMS spectra are acquired with TOF conditions optimized for photoion detection, while the SIMS spectrum is acquired with TOF conditions optimized for secondary ion detection. In the VUV-SNMS spectra, the dominant m/z = 130 feature corresponds to the methylene indole cation fragment. In panel (a) is also an image of the m/z = 130 feature, showing the spatial distribution of tryptophan (150 x 150 μm^2, 64 pixel x 64 pixel raster).

Figure 3: VUV-SNMS PIE curves of As_2 and Au_2 acquired with 100 ns of Bi_3^+ from ref [14] (•). The simulated PIE curves (for Au_2 T = 10 K (---) and T = 5000 K (—); for As_2 T = 10 K (---) and T = 4000 K (—)) are superimposed on the experimental curve. The method of simulation is discussed in the computational details section.

Figure 4: VUV-SNMS mass spectrum of tryptophan (50 ns of Bi_3^+, 100 scans) at 8.25 eV photon energy. The insert shows a magnified region around the parent mass at m/z = 204.

Figure 5: Relative energies, including zero-point energy corrections, of the tryptophan cation and the dominant fragments, calculated with B3LYP/6-311+G(d,p). The C-C bond that breaks upon fragmentation is indicated with the arrow.

Figure 6: VUV-SNMS of tryptophan (50 ns of Bi_3^+, 15 scans), in the mass range of m/z = 64-82 and m/z = 122-138, acquired with photon energies of 10 eV (a) and 8 eV (b). A stick spectrum illustrating the isotopic abundances of the methylene indole and deprotonated glycine radicals are shown in panel (c) for comparison.

Figure 7: Averaged PIE curves of thymine acquired via (a) VUV-SNMS and (b) thermal desorption, a total of four scans and two scans are used for the average, respectively. For each average, the individual PIE curves are normalized to each other at 9.2 eV, and total maximum changes between individual scans are shown via the grey shading. The experimental onsets, 8.74 eV for VUV-SNMS and 8.85 eV for thermal desorption, are indicated by the arrows. The same sample is used for both experiments.

Figure 8: Simulated photoelectron spectrum (see computational details section) of thymine. The $0\text{-}0^+$ transition is set at 0 cm^{-1}, and some major transitions are indicated (the vibrations are numbered in accordance to their frequencies in the cation). The calculated Franck-Condon overlap shows that the origin is the dominant transition in the photoionization of thymine between the two ground electronic states.

Figure 1:

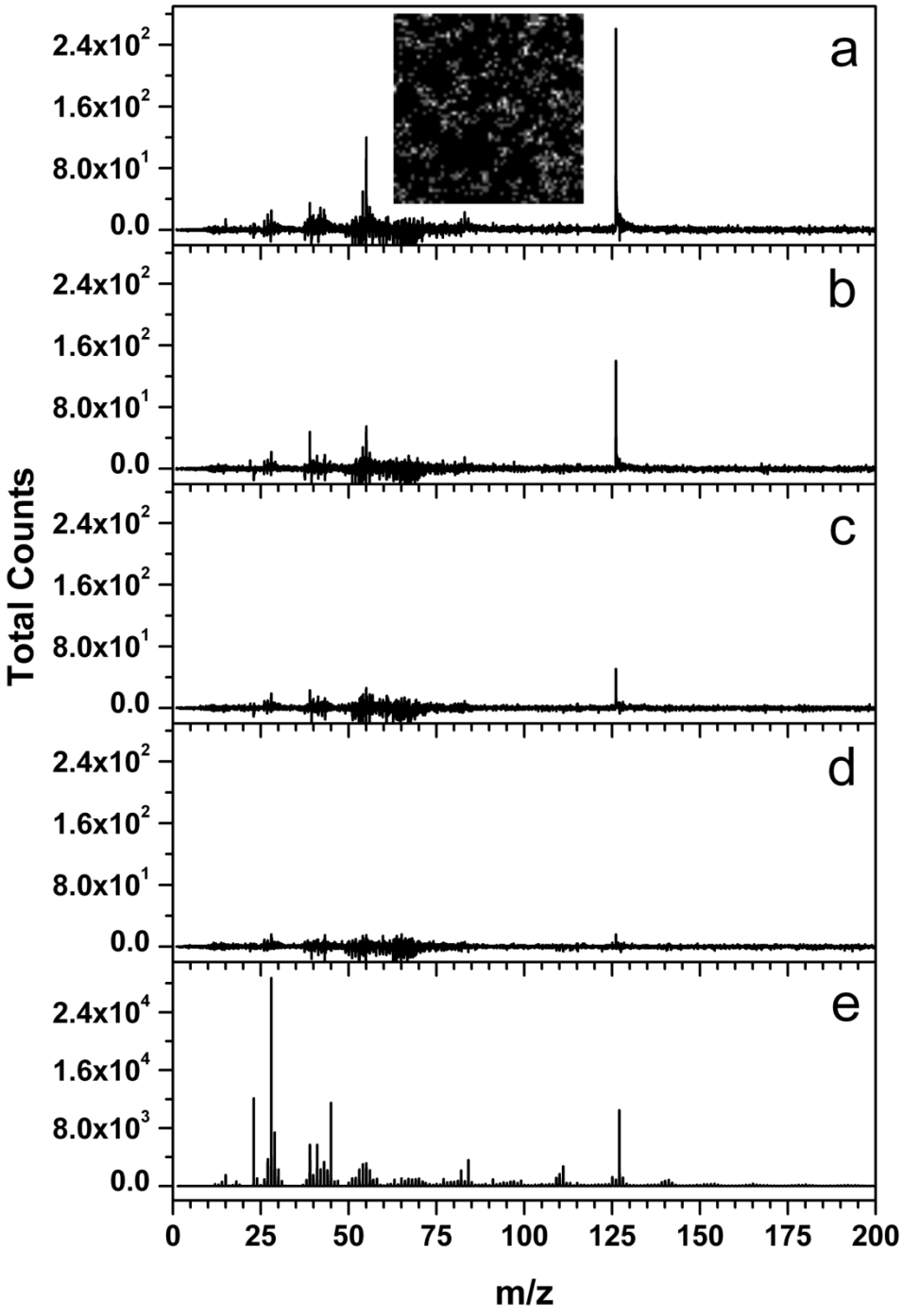
a
b
c
d
e
Total Counts
m/z
2.4x10^2
1.6x10^2
8.0x10^1
0.0
2.4x10^4
1.6x10^4
8.0x10^3
0
25
50
75
100
125
150
175
200

Figure 2:

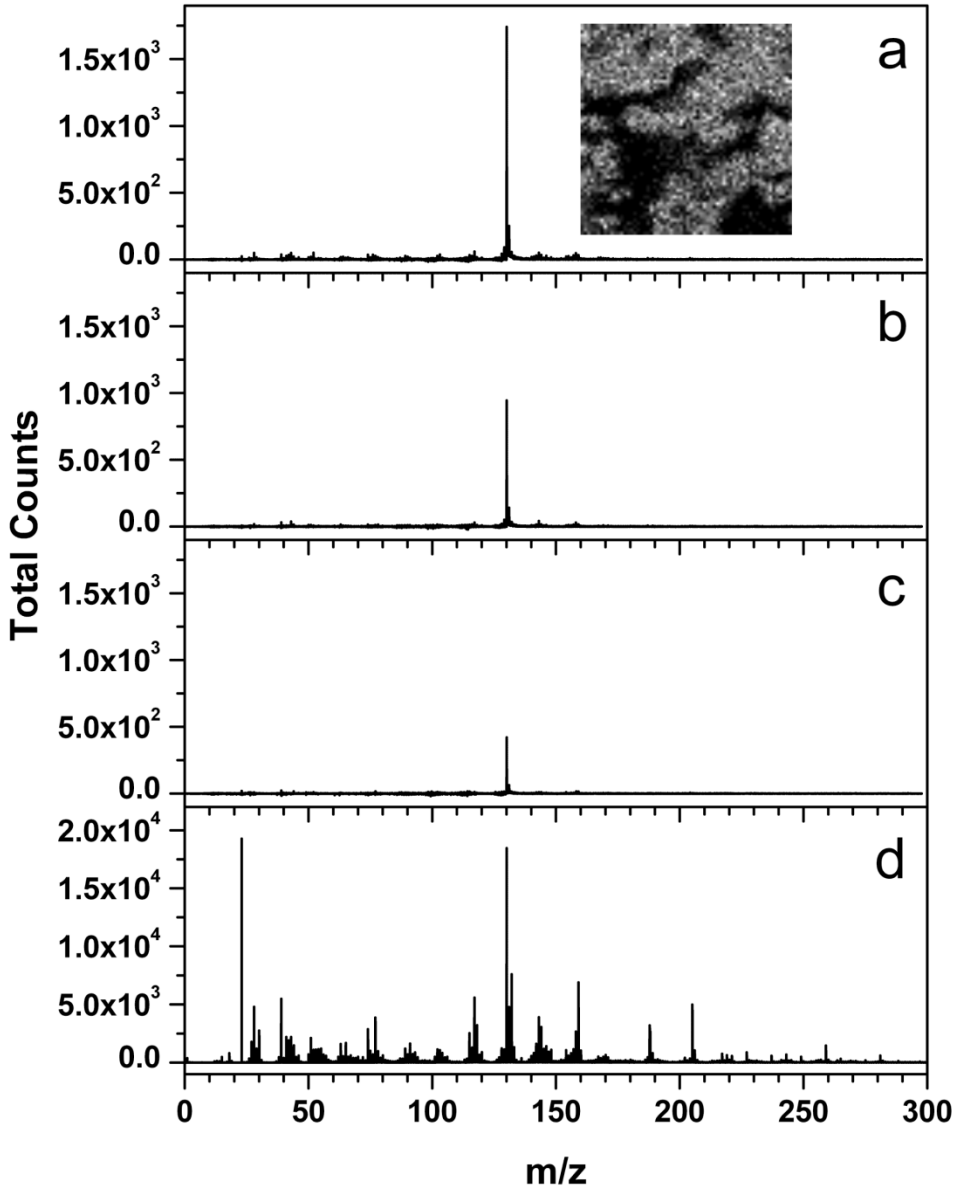
a
b
c
d
Total Counts
m/z
1.5x10^3
1.0x10^3
5.0x10^2
0.0
2.0x10^4
1.5x10^4
1.0x10^4
5.0x10^3
0
50
100
150
200
250
300

Figure 3:

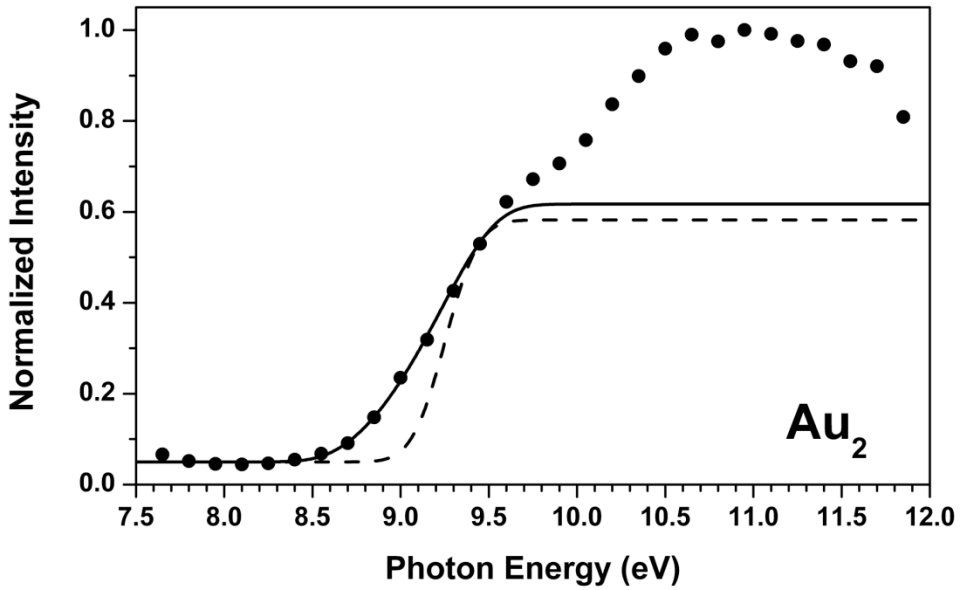
Normalized Intensity
1.0
0.8
0.6
0.4
0.2
0.0
7.5
8.0
8.5
9.0
9.5
10.0
10.5
11.0
11.5
12.0
Photon Energy (eV)
Au2

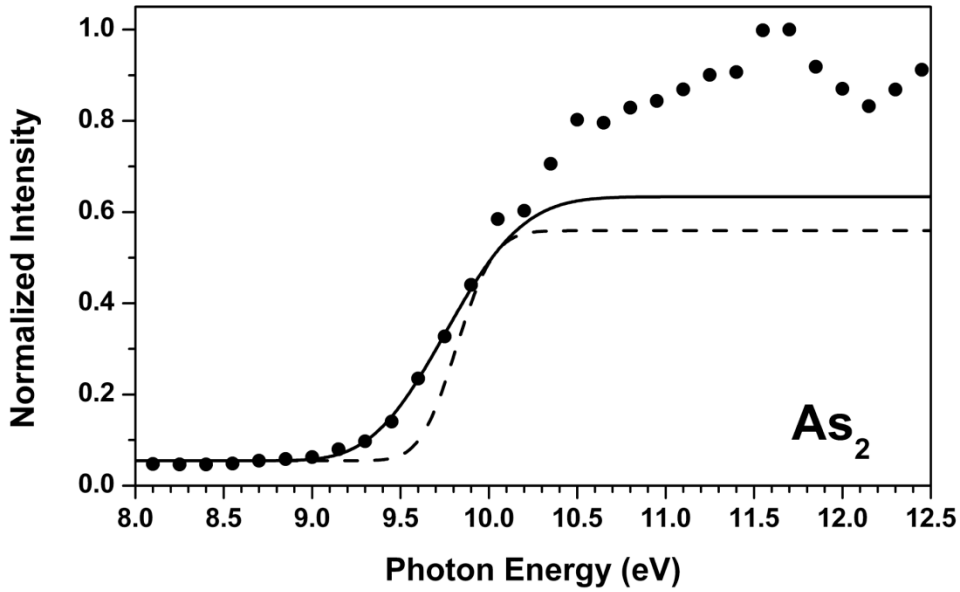
Normalized Intensity
1.0
0.8
0.6
0.4
0.2
0.0
8.0
8.5
9.0
9.5
10.0
10.5
11.0
11.5
12.0
12.5
Photon Energy (eV)
As2

Figure 4:

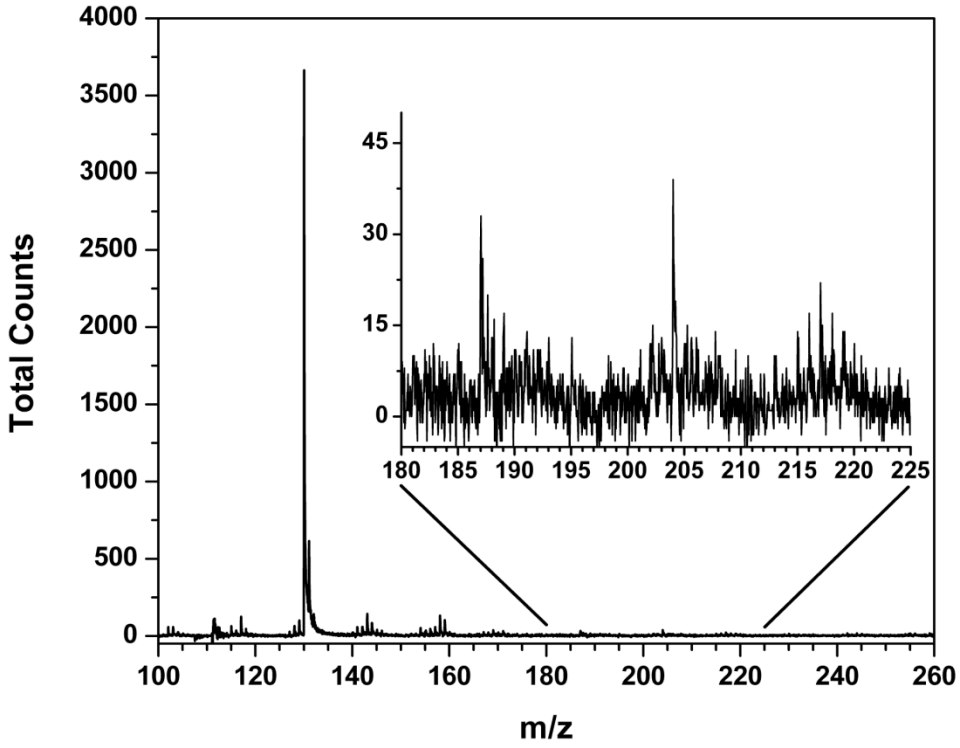
Total Counts
m/z
4000
3500
3000
2500
2000
1500
1000
500
0
100
120
140
160
180
200
220
240
260
45
30
15
0
180
185
190
195
200
205
210
215
220
225

Figure 5:

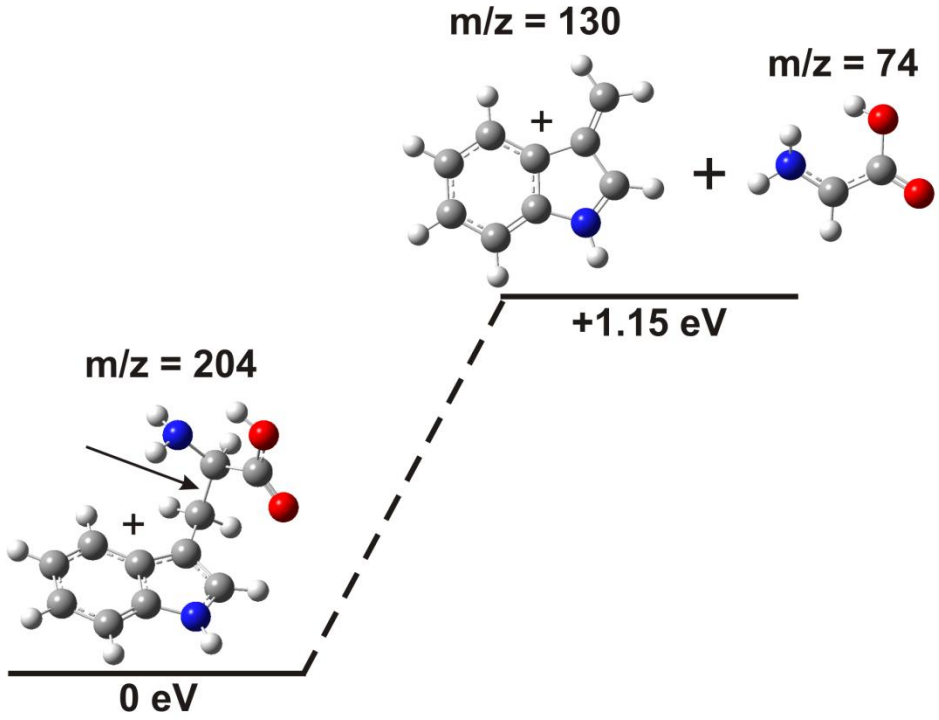

Figure 6:

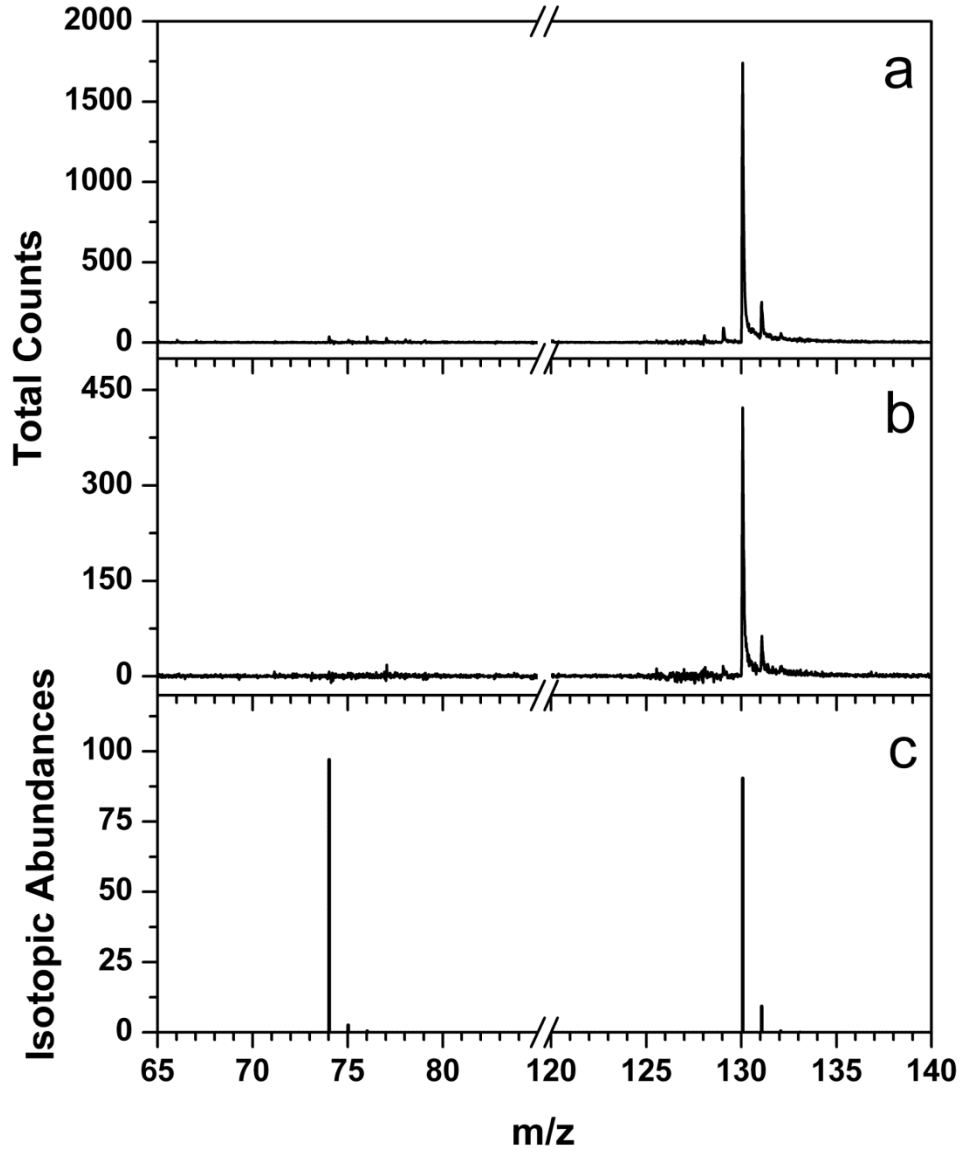
a
b
c
Total Counts
Isotopic Abundances
m/z
2000
1500
1000
500
0
450
300
150
0
100
75
50
25
0
65
70
75
80
120
125
130
135
140

Figure 7:

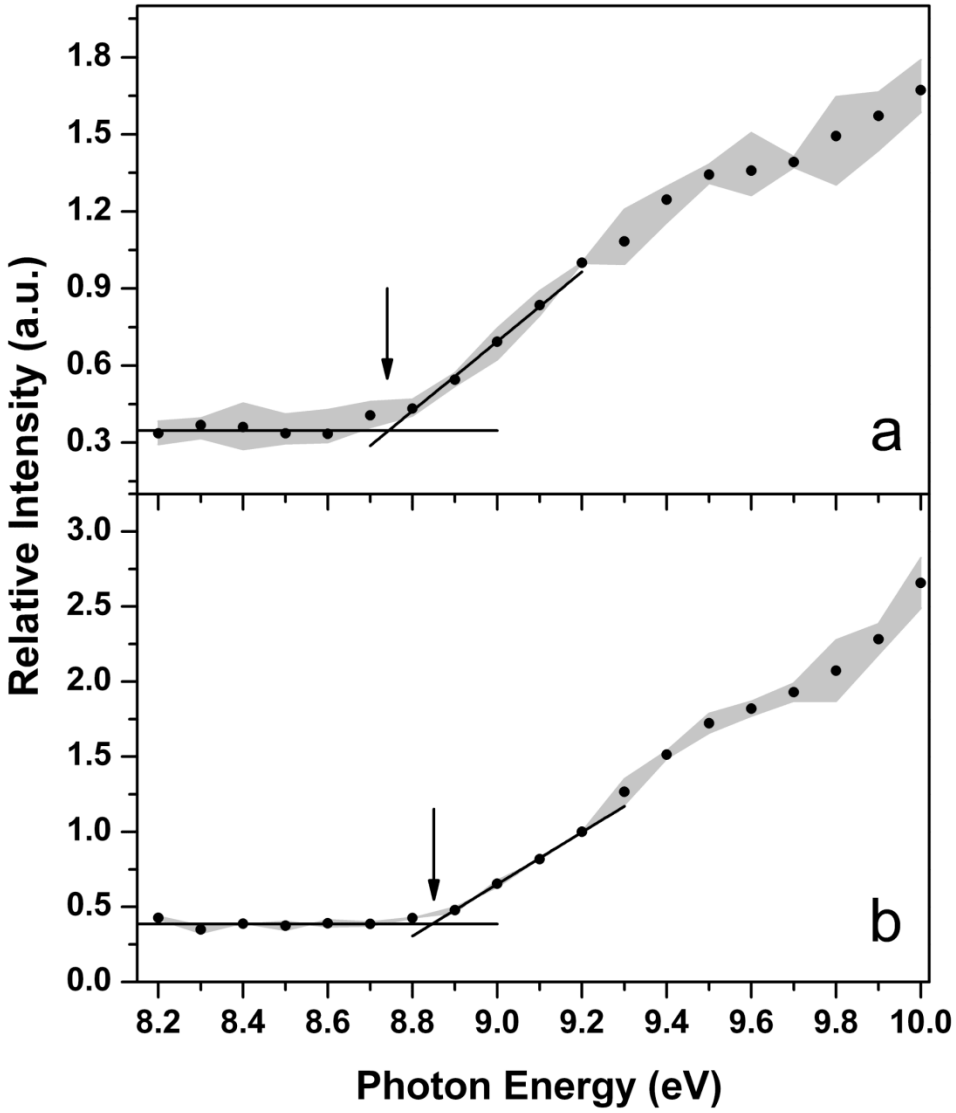
Relative Intensity (a.u.)
1.8
1.5
1.2
0.9
0.6
0.3
a
3.0
2.5
2.0
1.5
1.0
0.5
0.0
b
8.2
8.4
8.6
8.8
9.0
9.2
9.4
9.6
9.8
10.0
Photon Energy (eV)

Figure 8:

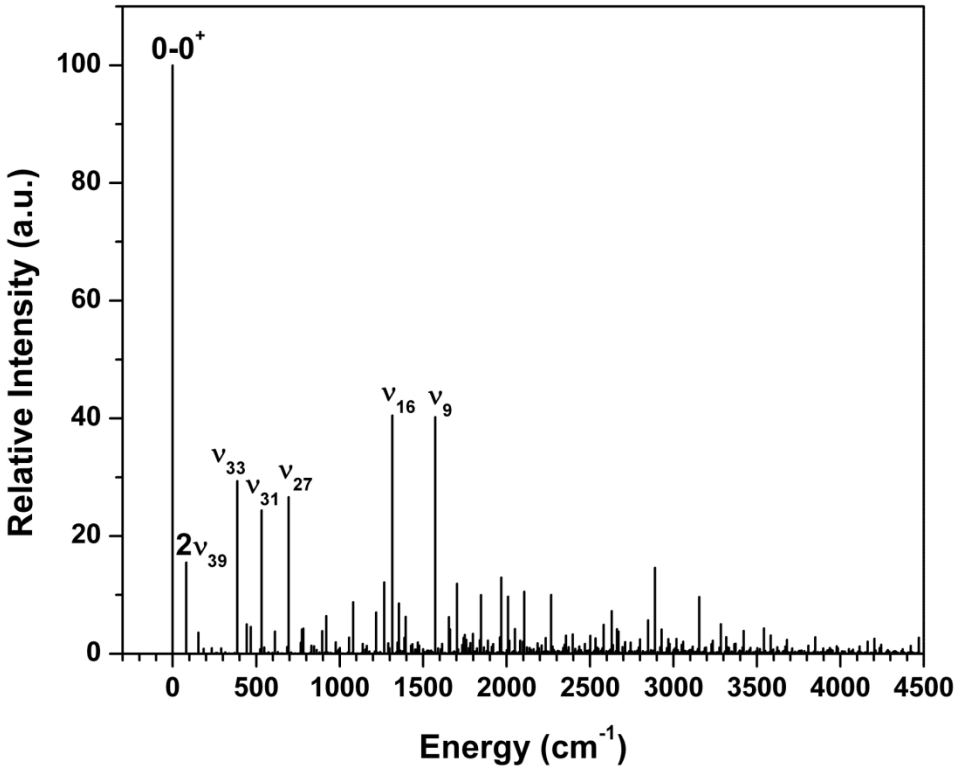
0-0+
100
80
60
40
20
0
Relative Intensity (a.u.)
2ν39
ν33
ν31
ν27
ν16
ν9
0
500
1000
1500
2000
2500
3000
3500
4000
4500
Energy (cm-1)